Structure investigation of nano-FeO(OH) modified clinoptilolite tuff for antimony removal

E. Chmielewská[a*], W. Tylus[b], M. Drábik[a], J. Majzlan[c], J. Kravčak[d], C. Williams[e], M. Čaplovičová[f], Ľ. Čaplovič[g]

[*a]*Faculty of Natural Sciences, Comenius University, Mlynská dolina, 842 15 Bratislava, Slovakia, e.mail: chmielewska@fns.uniba.sk*
[b]*Institute of Inorganic Technology, Wroclaw University of Technology, Wybrzeže Wyspianskiego 27, 50-370 Wroclaw, Poland*
[c]*Friedrich Schiller University, Chemical Geoscience Faculty, Institute of Geosciences, Burgweg 11, 07749 Jena, Germany*
[d]*Faculty of Electrotechnics and Informatics TUKE, Letná 9, 042 00 Košice, Slovakia*
[e]*University of Wolverhampton, School of Applied Sciences, Wulfruna Street,Wolverhampton WV1 1SB, United Kingdom*
[f]*STU Centre for Nanodiagnostics, University Science Park Bratislava Centre, Slovak University of Technology, Vazovova 5, 812 43 Bratislava, Slovakia*
[g]*Institute of Materials Science, Faculty of Materials Science and Technology, Slovak University of Technology in Bratislava, J. Bottu 25, 917 24 Trnava, Slovakia*

ABSTRACT

Biomimetic sol-gel synthesis was used to prepare new FeO(OH) zeolite (clinoptilolite tuff) adsorbent effective for antimony removal. The product was compared with other on the market accessible natural or commercial adsorption materials like granulated ferric hydroxide GEH, powder of zero valent iron (ZVI)-nanofer and the new synthesized oxi(hydr)oxide FeO(OH) and characterized by XRD, XPS, Raman, FT IR, TG, DTA, DTG, TEM and SEM techniques. Based upon the SEM analysis, the oxidized nanofer sample revealed the existence of hematite and goethite and morphology of FeO(OH) dopant confirmed the presence of ferrihydrite, in less extent also magnetite and hematite. Recorded exothermic maxima on DTA curves for powdered FeO(OH) zeolite at 460°C and for pure component FeO(OH) at 560°C indicated an 100°C shifted exothermic effect, which characterized strong chemical interaction of FeO(OH) with zeolite structure. Based upon the XPS analyses, also the difference between Fe species in the raw and FeO(OH) doped zeolite was found in increasing Si/Al ratio, however only at the surface below app. 5 nm, measured as 3.94 for raw and 5.38 for sample treated with alkalic solution. The plotting of adsorption isotherms in the system studied clearly showed the increasing uptake capacity of the adsorbents towards antimony with the increased S(BET) data (GEH >FeO(OH)>FeO(OH) zeolite>nanofer).

Keywords: Adsorption; FeO(OH) species; Goethite; Ferrihydrite; Magnetite; Hematite; Antimony removal

1. Introduction

Inspiration from nature has been widely used in the development of new materials and in the improvement of their properties since long time. Superhydrophobic surfaces inspired in species present in nature with highly water repellent self-cleaning properties, such as the well-known lotus leaf, are interesting examples of the biomimetic approach for the development of affordable materials and state-of-the-art techniques. The most progressive tissue engineering in regenerative medicine, gene therapy, drug encapsulation and other promising research results are known today [1-3].

Materials designed using components derived from biological sources such as collagen, chitosan, three-dimensional polymeric hydrogels like surfactants, alginate, plant proteins and

polysaccharides have also been investigated thoroughly for use in environmental adsorbents fabrication. Natural biomaterials possess some advantages over their synthetic counterparts, such as their capability to be environmentally viable and thus recognized by the living microenvironment. Since the beginning of 21st century, several types of hydrogels with excellent mechano-chemical properties have been developed through applying different synthesis routes. Biomimetic sol-gel strategy presents the most frequently used synthesis route in advanced adsorbents fabrication [4-6].

When iron is stored as a nanoparticle of iron oxide (ferrihydrite) inside the protein cage ferritin (Fn), it is completely sequestered and rendered inert. Thus the encapsulation and sequestration of the iron oxide nanoparticle in biological systems highlights its tremendous potential for use as a synthesis platform for material design. From understanding direct biomineralization in Fn, scientists developed a model for surface-induced metal oxide formation and have used this as a guiding principle for the synthesis of metal oxide nano-particles in other natural or engineered architectures [7-10].

Recent literature dealing with tectosilicates valorization reports state of the art mainly in their external surface modification using the sol-gel technique, surfactants coating, deposition of zero valent iron ZVI, silver clusters, iron oxihydroxide nanoparticles and semiconductor like titanium dioxide or their pelletizing with some biopolymeric eco-friendly carbohydrates [4-6,11-15]. Environmental requirements are becoming increasingly important in today´s society, since there is an increased interest in the industrial use of renewable resources. Simultaneously, it is believed that nature´s pattern may indicate that in the near future the synthesis development of traditional adsorbents might change.

Metal oxides based adsorbents are effective, low cost adsorption materials for heavy metals and other pollutants removal together with pathogen detection. Their sorption process is mainly controlled by complexation. When their particle size is reduced to below 20 nm, the specific surface area of normalized adsorption capacity increases 10– 100 times, suggesting a „nanoscale effect“. They may be combined with other carriers or pelletized or enriched with a broaden range of functional groups and thus separated magnetically. Current immobilization techniques usually result in significant loss of treatment efficiency. Therefore, research is needed to develop simple, low-cost methods to immobilize nanomaterial without significantly impacting its performance. Nevertheless, to overcome a potential human risk from environmental spreading, nanomaterials need to be embedded in a solid matrix, respectively, to have minimum release until they are disposed of [6,7,10,11].

Stibnite (Sb_2S_3) dominant mines were located in various zones of the Western Carpathians of Slovakia. All Slovak Sb deposits were closed and abandoned in the early 1990s mostly without their remediation. Unfortunatelly, this long-term exploitation of Sb has produced in country large amounts of waste rocks and tailings which are contributing to the contamination of the surrounded environment. Waters from each mine site show no acid drainage (pH 6.2-8.2) due to neutralizing by abundant Ca- and Mg-carbonate intercalations in the mineralized rocks. As analyses revealed, also substantial amounts of Sb is associated with hydrous ferric oxides (ferrihydrite and goethite) commonly occurring at that mines and thus helping to decrease this pollution. Despite the natural attenuation processes concentration of Sb in downstream surface waters and groundwaters are remaining high, many times overpassing the drinking water limit (5 µg/L). Antimony metalloid is considered to human health toxic and carcinogenic while elemental antimony is more toxic than its salts and inorganic forms are more toxic than organic ones [14].

Therefore, the objective of this work was to use zeolite (clinoptilolite tuff) from the inland deposit Nižný Hrabovec as template or nanoreactor in more effective biomimetic sol-gel synthesis and thus to prepare new upgraded, economically feasible adsorbent FeO(OH) zeolite. The adsorbent synthesized was characterized thermoanalytically, by TEM and XRD

and its FT IR, Raman, SEM micrographs and SEM-EDS records were compared with other similar products like GEH, nanofer, synthesized oxi(hydr)oxide FeO(OH) and parent (raw) zeolite. Finally, adsorption performance of the above materials towards antimony was validated by isotherms plotting.

2. Materials and methods

2.1. Adsorbents

Granulated ferric hydroxide (GEH^{104}), developed at the Department of Water Quality Control in Technical University Berlin, is an approved commercial adsorbent manufactured by GEH Wasserchemie GmbH & Co. KG Osnabrück (Germany). The main components of GEH are akaganeite (ß–FeOOH) and goethit [α-FeO(OH)]. The product has the specific surface area about 220 m^2/g, water content of 45%, bulk density 1.2 g/cm^3 and the price of 3750 Euro per ton [4-8,11].

The domestic zeolite (clinoptilolite tuff, deposit Nižný Hrabovec at the eastern Slovakia) was chosen on the base of its low-price availability in the local market (15-35 Euro per ton for size-granulation of 0.2 – 1 mm) and due to its sufficiently large surface area in powdered form (~ 60 m^2/g), the highest one among the other natural products, rigidity and surface functionality. The clinoptilolite tuff examined contains a significant percentage of the active mineral, i.e. clinoptilolite (cca 85 %) and is consequently classified as an excellent mineral cation exchanger. Mineralogical and chemical composition of the clinoptilolite tuff examined in this study describes literature [4,12] and Table 1.

Due to the very high price of commercial Fe-oxihydroxide (GEH) on our market which was quite frequently used for As and Sb removal from some underground water reservoirs in Slovakia we prepared and compared the chemically pretreated FeO(OH) clinoptilolite tuff with the above GEH product. Thus, 20 g of (0.2–0.8 mm) grain-sized zeolite was mixed with 0.5 L of 10 % aqueous solution of iron (III) nitrate nonahydrate [$Fe(NO)_3$. $9H_2O$, Alfa Aesar, crystalline, Germany] and aged at 60 °C in laboratory water bath shaker for 3 days. Then, the 200 mL of 2.5 M KOH solution was added dropwise to prepare the final suspension of pH = 12 and keeping it aged for another 6 days at room temperature. After the reaction period the suspension was filtered and washed with deionized water and finaly dried at 105 °C for 2 h in laboratory dryer.

Czech commercial product nanofer 25S (Nano iron, s.r.o, Rajhrad) was used for comparing the product adsorption capacity with all other examined samples due to some similarities with its iron oxides composition especially after air-oxidation and drying. Original nanofer substance as ZVI (Zero-Valent Iron) powder was stored and supplied in certified packaging. In order to prevent undesirable transformation of Fe(0) to Fe_2O_3 ZVI was processed in dispersing apparatus under protective atmosphere. The price of above product on the market is 26 360 €/ 1t.

2.2. Characterization

Elemental analysis of the samples and their SEM micrographs were performed on Scanning Electron Microscope SEM, Hitachi TM 3000 with integrated EDS spectrometer (EDS Oxford Instruments Swift ED 3000). Table 1b represents an average weight percentage

of the elements in individual sample calculated from 10-15 measurements depending on sample homogeneity.

TEM micrographs of FeO(OH) zeolite were visualized using a transmission microscope (TEM) JEM ARM 200cF working at 200 kV and by scanning electron microscope (SEM) JEOL JSM 7600F working at accelerating voltage 0.5 kV. The samples for SEM study were stuck on the double-sided adhesive tape and then carbon coated. Samples for TEM examination were firstly dispersed in ethanol using ultrasound and only a drop of suspension was placed on a carbon coated grid. After drying in the air, sample was studied in TEM.

The X-ray powder diffraction (XRPD) patterns were accomplished at room temperature on a BRUKER D8 Advance Apparatus with Cu antikathode, Ni K_{β} filters and LynxEye detector at 40 kV and 40 mA. The resulted patterns were compared with the JCPDS Cataloque (Joint Commettee on Powder Diffraction Standards No. 22-1236, 13-0304 for clinoptilolite).

For material characterization and structural investigation of the samples, the external surface area and porosity of clinoptilolite tuff including competitive samples were determined at liquid nitrogen temperature (76 K) on a Micromeritics ASAP 2400 Apparatus, using the static volumetric technique and t-plot methods with BJH pore diameter computation.

X-ray photoelectron spectral (XPS) measurements were carried out on the Specs Phoibos-100 hemispherical analyser operating at constant analyser energy mode in Wroclaw University of Technology. The measurements were performed at room temperature using 100W (wide scans) and 250W (narrow scans) of X-ray Mg anode. The base pressure in UHV chamber was below 2 x 10^{-10} mbar. The spectrometer energy scale was calibrated using the Au $4f_{7/2}$ and Cu $2p_{3/2}$. Sample charging was compensated by an electron flood at 0.5 mA current and 0.1±0.01 eV energy. The detection angle regarding the surface was normal. The powdered sample in the as received state was pressed into a molybdenum sample holder. The C1s peak of the carbon at 284.8 eV was taken as reference in calculating BEs and accounting effects. The spectra were collected and processed by SpecsLab software. Experimental peaks were decomposed into components (75% Gaussian, 25% Lorenzian) using a non linear, least squares fitting algorithm and a Shirley baseline.

FT IR spectra of FeO(OH) zeolite compared with other adsorption materials like GEH^{104} and commercial nanofer 25S were measured on FTIR spektrometer Nicolet 6700 (Thermo Scientific). In the IR region of 4000 – 400 cm^{-1} DTGS detektor and KBr beam divider were used. Measurements were done in transmission mode using the KBr tablets pressing (1 mg of sample was homogenized with 200 mg KBr). The spectral analyses were evaluated by means of program OMNIC.

The Raman spectra were acquired using dispersive Raman spectrometer JobinYvon Labram 300 in backscattering geometry with 80 x (NA = 0.75) long-working distance objective and a 632.8 nm HeNe laser with illumination power 17 mW.

Thermogravimetric (TG), differential thermogravimetric (DTG) and differential thermal analyses (DTA) were performed on SDT 2960, T.A.Instruments heating 100 mg of sample at 10 $^{o}C\ min^{-1}$ by the air atmosphere and in the temperature range 30 - 1000 ^{o}C. All samples were measured triplicate so that the graphical plots represent their average values. To

compare a potential thermoanalytical change between FeO(OH) zeolite grained and FeO(OH) zeolite additionally powdered, both samples were measured.

2.3. Sb adsorption

The stock solution of antimony was prepared from D.I. water and $KSb(OH)_6$ chemical acidified to pH = 2.6 with acetic acid to keep all the Sb species in aqueous solution dissolved. The pH control of all samples before and after the laboratory trials was carried out onto a WTW pH 3110 SET 2 instrument with SenTix ®R 41 electrode. Chemicals necessary for the stock solution preparation were purchased mostly from Lachema Brno (made in the Czech Republic) with analytical grade quality. In the Sb solution under such pH, species as undissociated $Sb(OH)_3$, SbO^+, $Sb(OH)_2^+$, H_3SbO_4 and H_3SbO_3 may occur, which means that antimony is present predominantly in Sb(III) valency. Due to a sufficient low pH of initial solution, after the equilibration trials the pH of model Sb solutions did not increase over the value 2.7 as well as any turbidity appeared and samples remained visually clear. Moreover, to exclude a potential colouring of the tested Sb solutions with Fe species, all samples incl. FeO(OH) zeolite were thoroughly washed in D.I. water and dried before examination. Sb concentration in all water solutions was analysed on AAS instrument ZEEnit 700 in cooperation with Zeocem Company, Bystré (Slovakia).

Continuous and well mixed batch reactor used to be most common way to study the reaction between solute and adsorbent. Batch mode or discontinuous adsorption experiments were carried out using the 30 mL aliquot of model solution with variable pollutant concentration and 0.3 g adsorbents (weight with analytical precision) equilibrated for the designated time interval in 50 mL polyethylene centrifuge tubes, after which the supernatant solutions were separated mostly by centrifugation or through 0.45 μm membrane filter and such rezidual pollutants analysed. The samples were agitated by constant speed (180 rpm) using the Biosan SIA Multi-Rotator (Multi RS-60, Latvia). From Zeocem Company obtained zeolite in size granulation 0.2 – 0.8 mm was sieved and only the range 0.2 – 0.5 mm separated for examination and thus unified with other samples of GEH, nanofer and FeO(OH) in order to provide better mass uptake and to adjust it to the small volume of the used rotator tubes as well as volume of Sb solutions (30 mL). All measurements were done triplicate.

The equilibrium uptake capacity a (in mg/g) for each sample was calculated according to following mass balance equation:

$$a_{eq} = \left(\frac{C_i - C_{eq}}{m} \right) V$$

where c (i) and c (eq) were initial and equilibrium concentrations of studied pollutant (in mg/L), m was the mass of adsorbent examined (in g) and V was volume of the solution in liters (L).

3. Results and discussion

3.1. Characterization

3.1.1. SEM-EDS, morphology and TEM studies

According to Table 1 the SEM-EDS analyses confirmed the highest Fe content in the nanofer sample, however in the examined state it had already oxidized to various phases of iron oxides, mostly hematite Fe_2O_3 and magnetite Fe_3O_4 (68.1%), then the GEH sample indicated 51.88% of Fe total and the third position belongs to FeO(OH) (14.69%). The FeO(OH) zeolite indicates about 6%. This sample in regard to its parent (raw) zeolite (about 1% of Fe total) enriched the Fe content to sufficiently high level to be able to remove a broad variety of pollutants from contaminated water [8,10,15,16]. Separately sythesized iron oxi(hydr)oxide, denoted here as FeO(OH), possess extra high oxygen content indicating a potential mixture of iron oxides and potassium as well, due to KOH solution, which was applied during the synthesis to provide high pH and thus keeping iron oxi(hydr)oxide precipitation. The iron content of this sample was found to be 14.69%. No other point of interest can be seen in Table 1 from the identified and quantified elements.

SEM micrographs of the studied samples, as complementary investigations, visualize typical morphologies of individual adsorbents (Fig. 1). FeO(OH) clinoptilolite tuff outlines the boundary of a pore filled with more or less tabular, euhedral crystals of clinoptilolite, which are small and in some cases coated with a thin sheet of authigenic clay. Over this SEM various phases of iron oxides (FeO(OH), GEH, nanofer) reveal small inclusions filled with iron oxides. Some crystal habits of iron oxide are seen round or disc-shaped hematite coordinating rod-shaped goethite. Dark areas are dominantly goethite, whereas light areas are hematite. The oxidized nanofer displays also potential magnetite with morphology of hexagonal prism shape. Metastable ferrihydrite is known to be a precursor of more crystalline hematite and goethite and generally exists as a fine grained and highly defective nanomaterials with flake-like morphology (the third SEM downwards). The SEM micrographs correspond with several other published results dealing with iron oxides immobilization and visualization [7,8,16].

Table 1
An average mineralogical and chemical composition of the clinoptilolite tuff (raw zeolite) from the deposit Nižný Hrabovec (a); An average weight percentage of the elements composing the studied samples by SEM-EDS (b).

Species	wt.%
clinoptilolite	70-85
volcanic glass	15-20
feldspar	7-10
cristobalite	2-4
alfa-quartz	2-3

oxides	wt.%	metals	wt.%
SiO_2	67.16	Zn	0.0024
Al_2O_3	12.3	Ba	0.0353
CaO	2.91	Pb	0.001
K_2O	2.28	Sr	0.01
Na_2O	0.66	Cs	0.0004
Fe_2O_3	2.3	Cr	0.0008
MgO	1.1	Cu	0.0002
P_2O_5	0.11	Ni	0.0001
MnO	0.14	Co	0.0001
TiO_2	0.17	Cd	0.00005
H_2O	10.9	Fe	0.9
		Ag	0.003

a)

Raw zeolite (clinoptilolite tuff)

Element	Weight %	Error(±)
Oxygen	57.880	1.320
Magnesium	0.417	0.052
Aluminum	5.163	0.153
Silicon	27.320	0.647
Potassium	2.052	0.094
Calcium	1.435	0.078
Iron	1.013	0.098

Nanofer 25S

Element	Weight %	Error(±)
Oxygen	27.899	0.255
Sodium	1.683	0.134
Aluminum	0.528	0.071
Silicon	1.825	0.076
Iron	68.066	0.276

Granulated oxohydroxide GEH

Element	Weight %	Error(±)
Oxygen	43.348	0.356
Aluminum	0.439	0.074
Silicon	0.822	0.075
Chlorine	1.683	0.085
Iron	51.880	0.363
Antimony	1.828	0.192

FeO(OH) zeolite

Element	Weight %	Error(±)
Oxygen	55.954	0.385
Magnesium	0.383	0.055
Aluminum	5.054	0.090
Silicon	25.075	0.238
Potassium	4.170	0.120
Calcium	0.840	0.090
Iron	5.817	0.237

FeO(OH)

Element	Weight %	Error (±)
Oxygen	59.800	0.318
Sodium	0.399	0.089
Potassium	25.115	0.217
Iron	14.687	0.247

b)

TEM micrographs in Fig.2 are simultaneously compared with more detailed SEM visualization in order better recognize surface coating of clinoptilolite tabular crystals with FeO(OH) hydrogels. Clusters (some flaky precipitate) of Fe-species in TEM micrographs clearly show their nano size and their localization inside the accessible space of various interparticle voids.

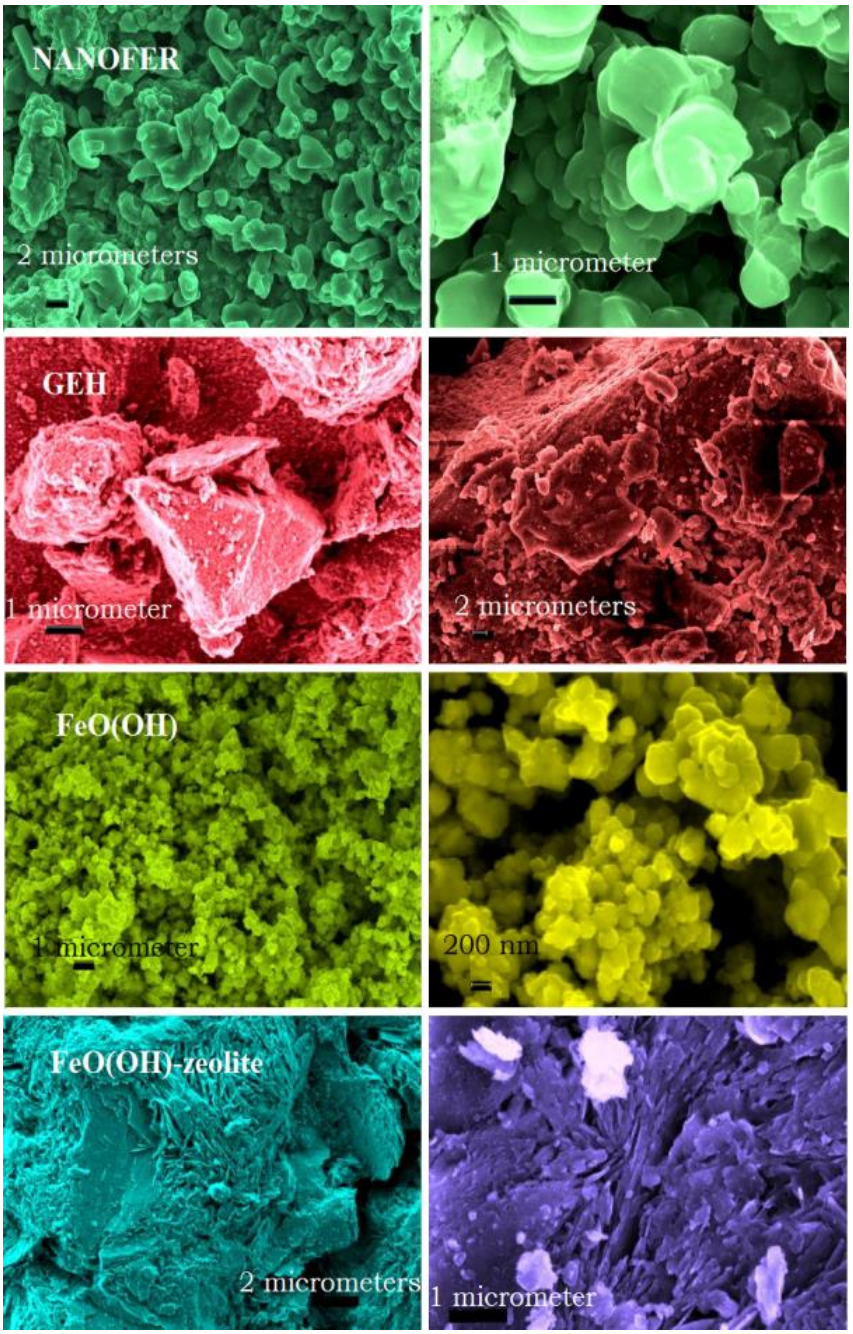

Fig. 1. Scanning Electron Micrographs of nanofer, GEH, FeO(OH) and FeO(OH) zeolite (downwards).

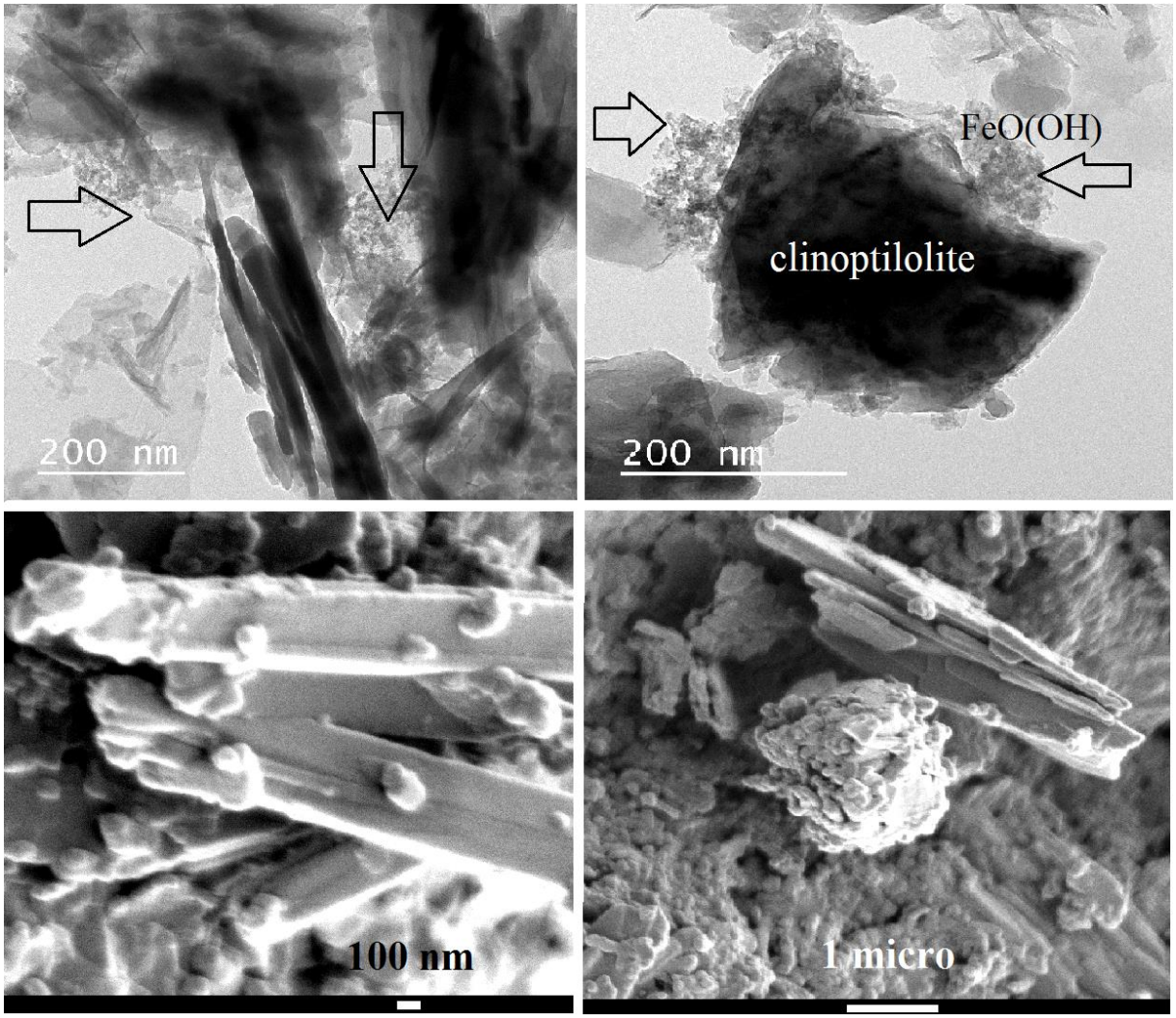

Fig.2. TEM (upper part) and SEM (lower part) micrographs of FeO(OH) zeolite**.**

3.1.2. XRD and S(BET) analyses

Material control and physical inspection of natural zeolites starts basically with X-ray diffraction (XRD). After treatment of the raw zeolite with highly alkalic iron nitrate solutions, the XRD measurements did not reveal any clinoptilolite matrix destruction or enrichment with a new Fe crystalline phase (Fig.3, upper record). All recorded diffractometer traces are typical for well crystallized clinoptilolite corresponding with d – spacings. The characteristic Braggs reflections at 10, 22 and in the range 25 – 30 of 2 theta are well observed. It is supposed that the new immobilized FeO(OH) hydrogels onto zeolite rock in form of amorphous phase with the content below 10 wt.% might result in not detectable change of both X-ray diffractograms.

Based on SEM, XRD (Fig.3, lower plot) and S(BET) measurements, it was supposed that the new synthesized iron oxi(hydr)oxide resembles mostly ferrihydrite [1-3], it has a verified S(BET) = 148 m^2 g^{-1}. The producer of GEH in the Company Datasheet a S(BET) value equalled to 298 m^2 g^{-1}. Despite the embedded nanodispersed FeO(OH) hydrogels into the mesoporous structure of zeolitic rock (2-50 nm), the S(BET) of this product remained rather similar with its raw counterpart (35.6 m^2 g^{-1}) – Table 2.

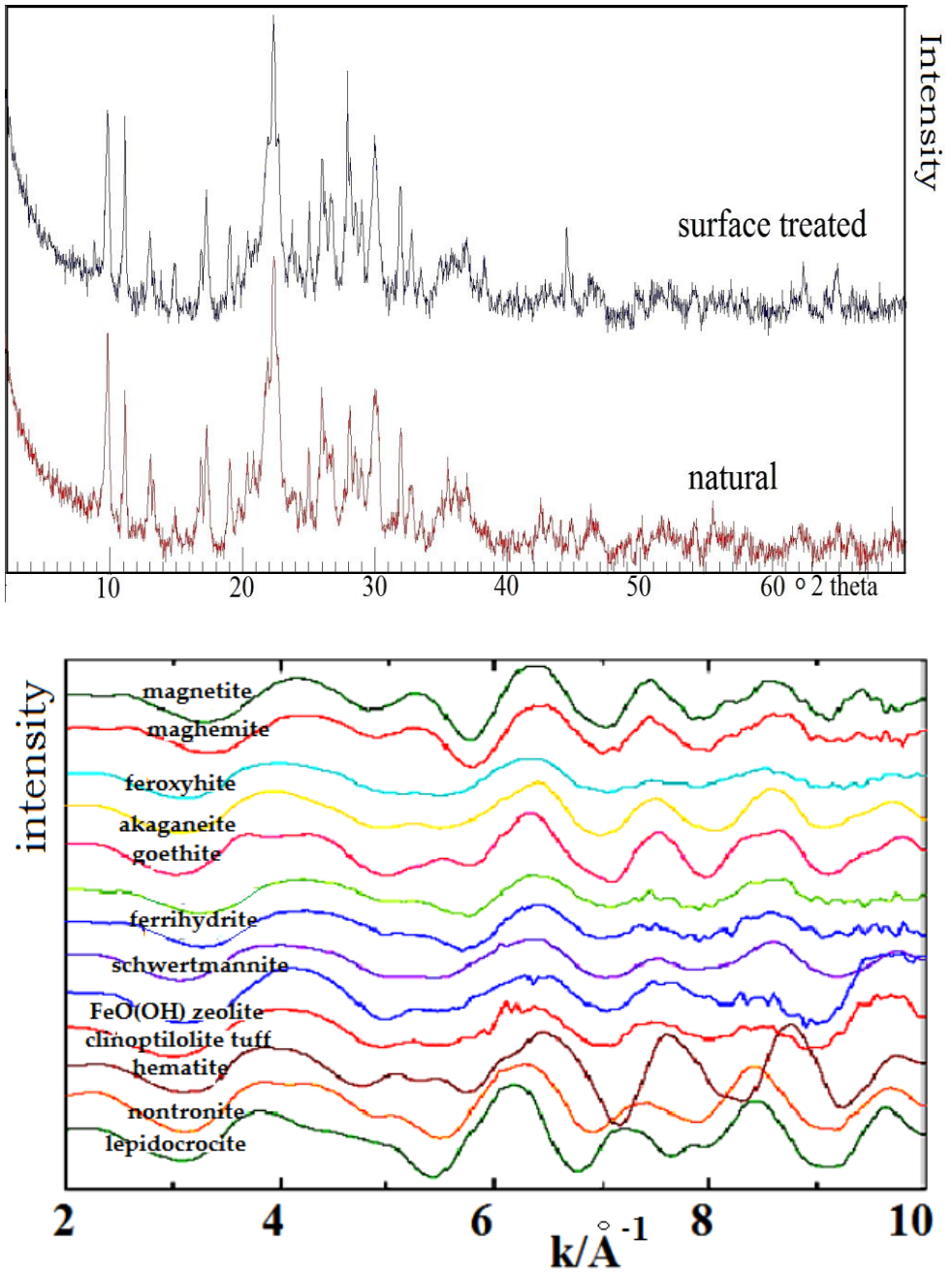

Fig. 3. X-ray diffractograms of natural and FeO(OH) treated zeolite (upper record) and comparison of X-ray diffractograms for other Fe minerals (lower plot).

Table 2
Specific surface areas and porosity values of the adsorbents studied.

Sample	S_{BET} (m^2/g)	S_t (m^2/g)	V_{micro} (cm^3/g)	BJH (nm)	Va
Clinoptilolite tuff (Nižný Hrabovec)	31.7	21.4	0.0045	14.5	0.106
FeO(OH) zeolite	35.6	31.4	0.002	13.8	0.135
FeO(OH) ferrihydrite	148	150	0	3.2	0.117
Nanofer 25S	25	22.2	0.001	11.8	0.074
GEH[104] (granulated ferric hydroxide)	298	299	0	3.7	0.324

S(BET) - active surface area determined by nitrogen adsorption and BET isotherm
S(t) - surface area of mesopores & external surface area determined by t-plot method
V(micro) - volume of micropores determined by t-plot method
BJH - average pores diameter according to Barrett, Joyner and Halenda
Va - total volume of adsorbed nitrogen calculated according to $p/p_0 = 0.99$

3.1.3. XPS investigations

Studies of zeolite surface phenomena and their surface microtopography by means of XPS ultra high vacuum technique became well established in the recent years. Such a surface analytical and thin film technique enables to investigate not only quantitative elemental composition of solid surfaces including surface Si/Al and bulk Si/Al ratio, important in zeolite chemistry, but also various diffusion, oxidation and other processes and reactions ongoing onto zeolite, concentration and distribution profiles of the host species, microstructural irregularities, surface interfaces and their bounding energies (BE) [18]. Binding energies, as the Figs. 4a,b illustrate, were element specific, containing chemical information due to dependence of the core electron energy levels on the chemical state. Usually, the BE increased with the increasing of oxidation state or electronegativity of element. The situation of iron in clinoptilolite structure is particularly interesting because this element can be either as an extra framework cation in the clinoptilolite cavities or like Al substituting Si atoms in the tetrahedral positions of its framework. Therefore, XPS analyses were performed to provide information about the chemical state of Fe cations in the zeolite samples, both in raw one as reference sample and FeO(OH) doped one, respectively. Fig.4c shows the XPS spectra of FeO(OH) doped zeolite in the binding energy region as the observed Fe $2p_{1/2}$ and Fe $2p_{3/2}$ doublet, fitted by two Gaussian functions and centered at energy binding of 726 eV and 713 eV, respectively. The binding energy of the Fe $2p_{3/2}$ signal was shifted to higher energy compared with value 711.6 eV, which used to be reported for this peak in Fe_2O_3 compounds [18] due to the influence of Al atoms in the clinoptilolite matrix. Furthermore, Fe_2O_3 from the surface and generally Fe(III) were potentially reduced to FeO and Fe(II) during the Ar sputtering, because the surface of the zeolite was etched twice with Ar^+ (BE range of Fe 3p was shifted to about 0.75 eV lower values, respectively) – Table 3. There were confirmed also differences between Fe species in the raw and FeO(OH) zeolite in increasing surface Si/Al ratio, measured as 3.94 for raw and 5.38 for sample treated with alkalic solution of $Fe(NO_3)_3$, however based on XPS technique only below approximately 5 nm from the outer surface. Some small Al leaching (0.14 wt.%) from surface structure may not be excluded due to alkalic treatment of zeolite. Oppositely, according to SEM-EDS values (Table 1) calculated bulk Si/Al ratio dropped from 5.3 to 4.98. Extra framework cations like Mg^{2+} and Ca^{2+} from the external surface were substituted with K^+ ions, that were enriched into the cavities from the applied KOH solution during the pretreatment procedure (Table 1). Despite to this alkalic treatment, as previously mentioned, XRD analysis of FeO(OH) doped zeolite did not confirm any breakdown of its structure. Some remaining part of iron species may get adsorbed onto the surface of zeolite (supposing below 5 nm deep outer layer) too, mainly in Fe(III) valency as Fe_2O_3.

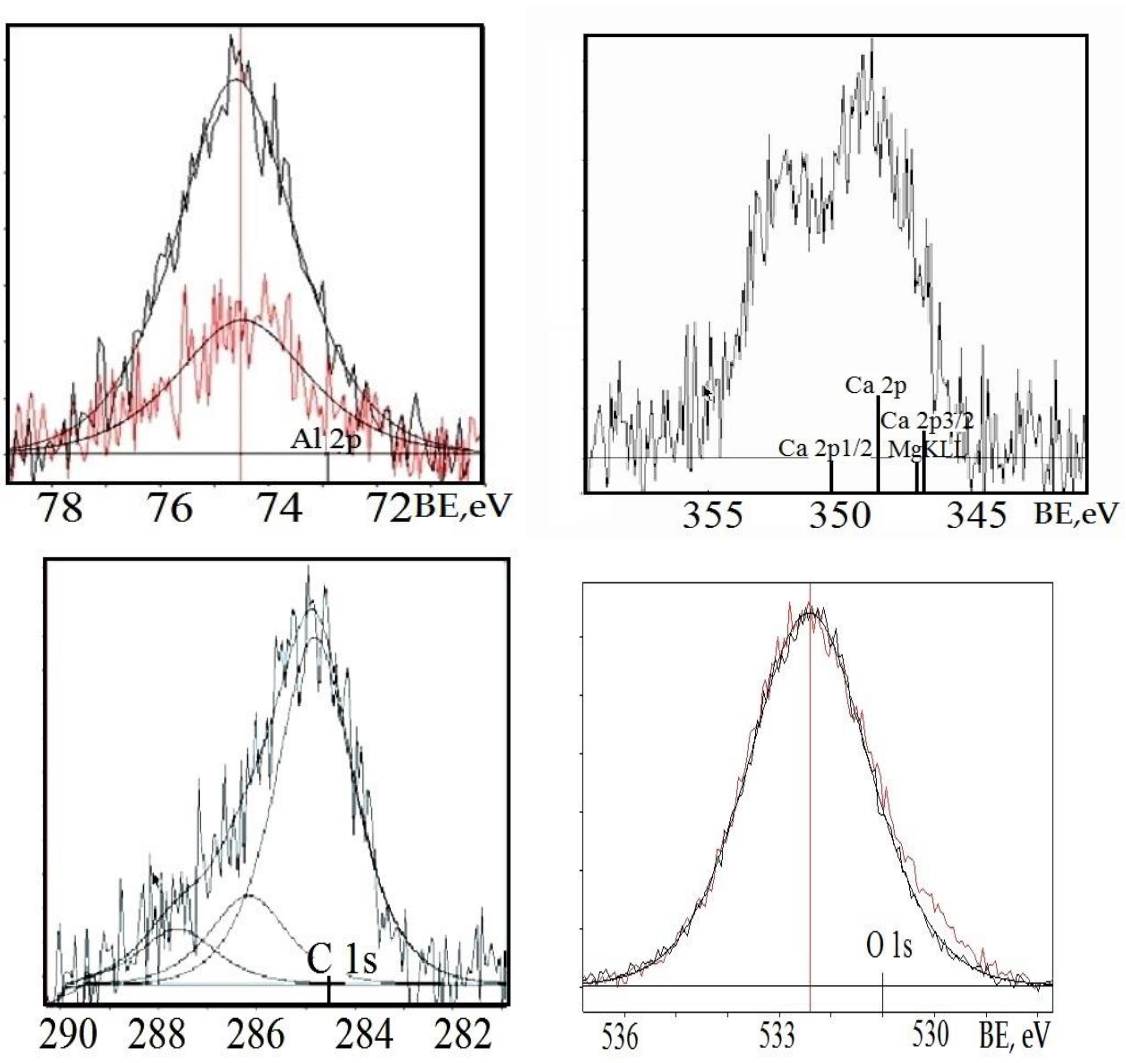

Fig. 4a. XPS Al 2p, Ca 2p, MgKLL, C 1s and O 1s of raw (black line) and FeO(OH) zeolite (red line) (from the left to the right downwards).

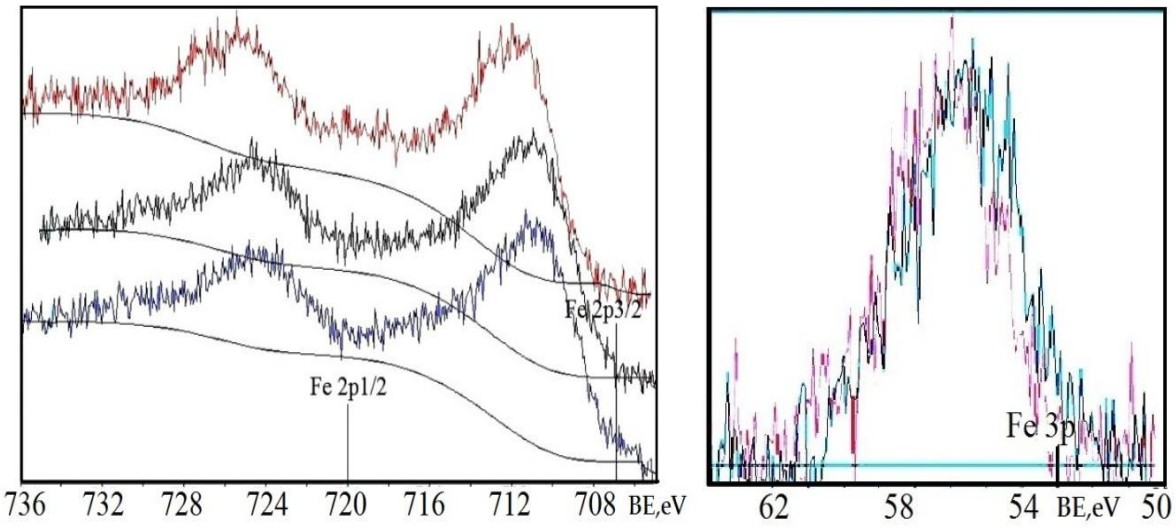

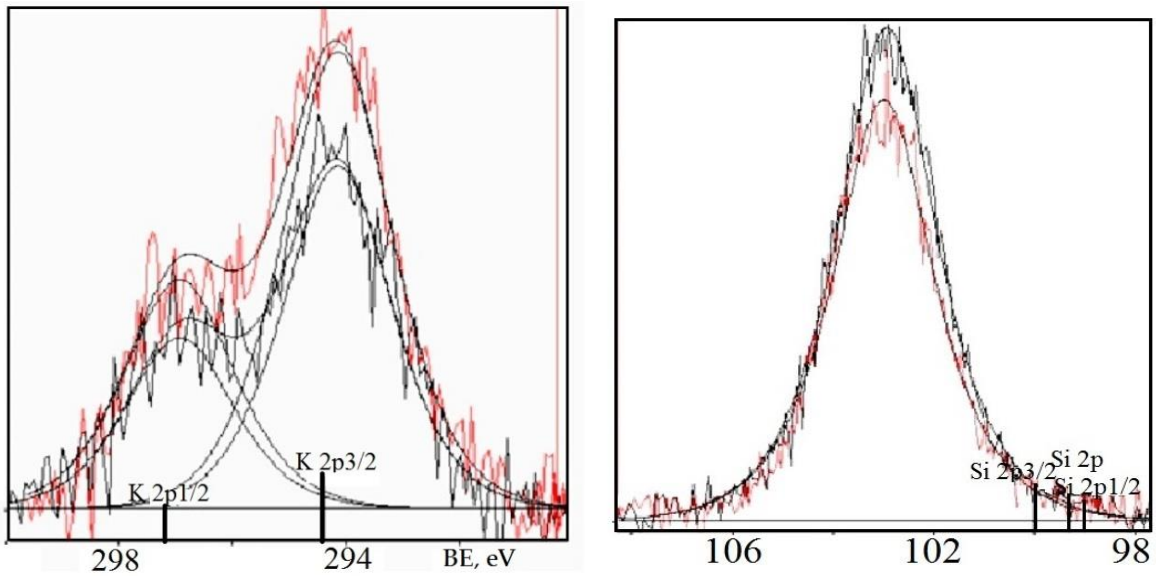

Fig. 4b. XPS Fe 2p1/2, Fe 3p, K 2p3/2 and Si 2p of raw (black line) and FeO(OH) – zeolite (red line) (from the left to the right downwards).

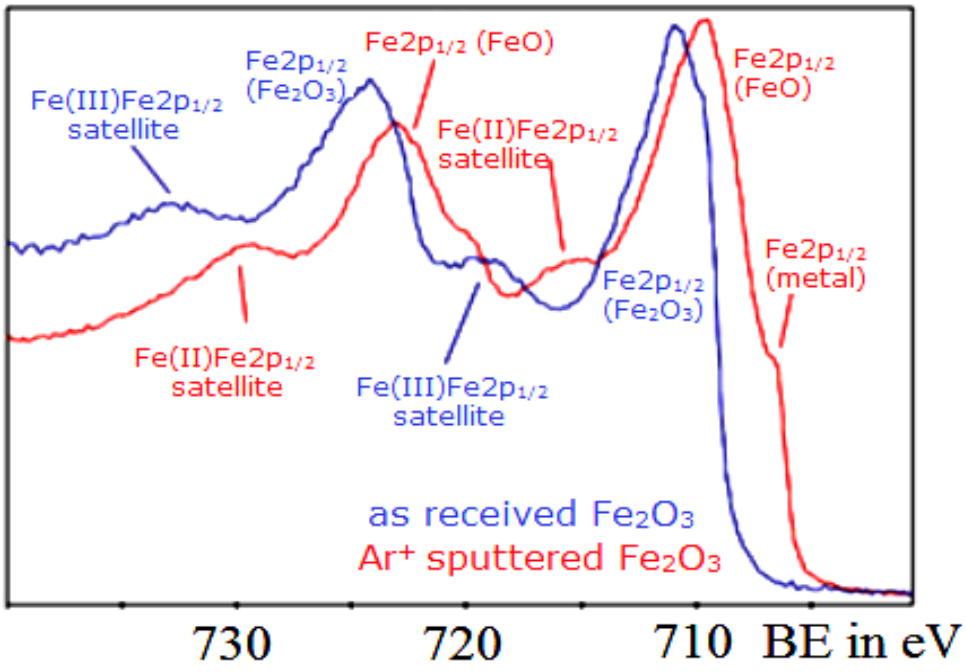

Fig. 4c. Distinquished Fe oxidation states in FeO(OH) zeolite using XPS analysis and satellite features of Fe2p.

Table 3
Binding energies of the elements composing the raw and FeO(OH) doped zeolite determined by XPS.

Element	Raw zeolite (eV)	FeO(OH) zeolite (eV)
O 1s	532.43	532.43
Si 2p	102.93	103
Al 2p	74.6	74.48
Mg KLL	346.9	-
K $2p_{3/2}$	294.14	294.15
Ca $2p_{3/2}$	348.5	-
C 1s	284.8	284.8
Fe $2p_{1/2}$	726	725
Fe $2p_{3/2}$	713	711.6
Fe 3p	55.25	56

3.1.4. FT IR and Raman spectroscopy analyses

As Fig.5 shows, FT IR spectra of raw clinoptilolite tuff and tuff enriched with FeO(OH) have characteristic absorption bands in the middle IR range between wavenumbers of 200 – 1300 cm^{-1}, observed typically as stretching vibrations of aluminosilicate tetrahedras. The bands at 1630 to 3690 cm^{-1} are due to trace of water in the samples cavities. Spectrum of the new synthesized FeO(OH) zeolite (in Fig.5 the 3th spectrum downwards) displays also some characteristic peaks at wavenumbers 3448 and 455 - 467 cm^{-1}. However, the FT IR spectrum did not reveal occurrence of some additional crystal phase of Fe oxide in FeO(OH) zeolite, probably due to overlapping of characteristic bands for Fe-O at wavenumbers 490, 599, 1370 and 1580 cm^{-1}. Sharp absorption bands at wavenumbers 3438 to 3443 cm^{-1} by GEH, nanofer and pure FeO(OH), however also by FeO(OH) zeolite but with some desreasing extent and shiffted to a higher wavenumbers, may indicate physico-chemical surface hydroxylation with O-H...O groups. By nanofer the absorption band at 575 – 581 cm^{-1} identifies potentially magnetite Fe_3O_4. There is supposed that vibrations at wavenumbers 795 to 796 cm^{-1} by raw and also by FeO(OH) zeolite characterize skeletal, crystal - bound Fe(III) oxide, content of which in raw zeolite is recorded as cca 1%. Wavenumbers at 1624 – 1637 cm^{-1} and 467 -470 cm^{-1} in both types of samples indicate probably hematite (Fe_2O_3).

Also Raman spectra were measured on specific individual samples. As seen from the spectrum in Fig. 6, oxidized nanofer displayed structural phase conversion when exposed to focused laser irradiation (to high excitation power with more then 7 mV). It recrystallized to a lower valency iron oxide closed to that occurring in GEH product, i.e. from magnetite to akaganeite. According to literature [16,17] morphology and composition of the particles obtained by laser irradiation suggest that iron oxide particles might get melted. As observed in Fig.6, the spectra of FeO(OH) zeolite, GEH and oxidized nanofer, except FeO(OH), remained quite similar. Characteristic bands near 670 cm^{-1} and 300 cm^{-1} may be assigned to magnetite and bands around 600, 400, 280 and 220 cm^{-1} to hematite [17].

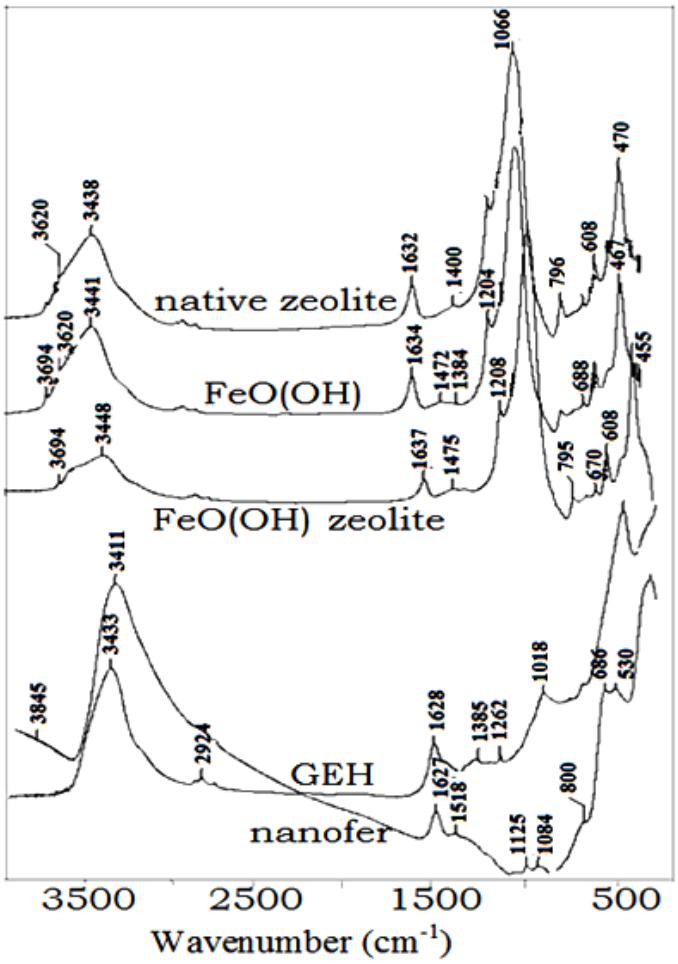

Fig.5. FT IR spectra of FeO(OH) zeolite compared with samples of GEH, nanofer, native zeolite and synthesized FeO(OH).

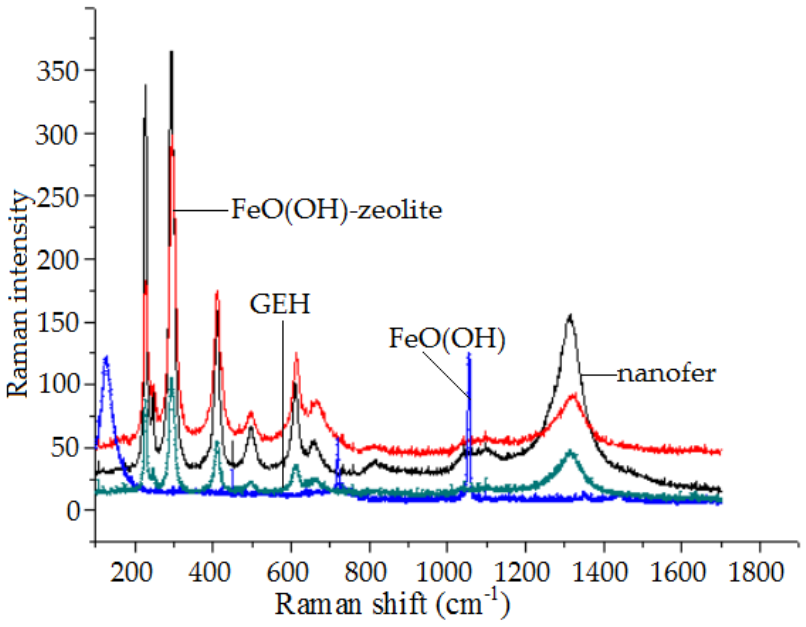

Fig. 6. Raman spectra of adsorbents studied.

3.1.5. Thermal analyses

According to the thermoanalytical measurements the sharp endothermic minimum was observed on DTA curves with raw zeolite at 95.94°C, however with the FeO(OH) zeolite at cca 0.7°C higher temperature - 96.63°C (Fig.7). On the other hand, second appearing endothermic minimum by the raw tuff was observed at 500.55°C, while by FeO(OH)-treated zeolite was that peak forwarded to temperature 458.02°C and especially its parent powdered sample showed here clear exothermic maximum. Until this temperature the examined sample lost ca. 9.6% of the weight. First shifting of endothermic minimum to higher temperature by FeO(OH) zeolite means a higher water content in the sample after FeO(OH) doping (Fig.7 upper right). Supposing that doped Fe(III) element substituted Al(III) atom in AlO_4^{5-} - tetrahedras of zeolite matrix or destroyed some surface AlO_4^{5-} - tetrahedras, the crystal structure of FeO(OH) zeolite started to break down earlier at the temperature 458.02°C. Also 2 recorded exothermic maxima on DTA curves, for powdered FeO(OH) zeolite at 460°C and for pure component FeO(OH) at 560°C, indicated an 100°C shifted exothermic effect which characterized strong chemical interaction of FeO(OH) with zeolite structure. Simultaneously, around the temperature 500°C might the doped FeO(OH) hydrogels recrystalize to microcrystalline hematite Fe_2O_3 (magnetite is stable only till 200°C) [11,15]. In regard to raw zeolite the FeO(OH)-treated zeolite recorded in DTA curve at 969.85°C some small endothermic effect, respectively (Fig.7 lower right).

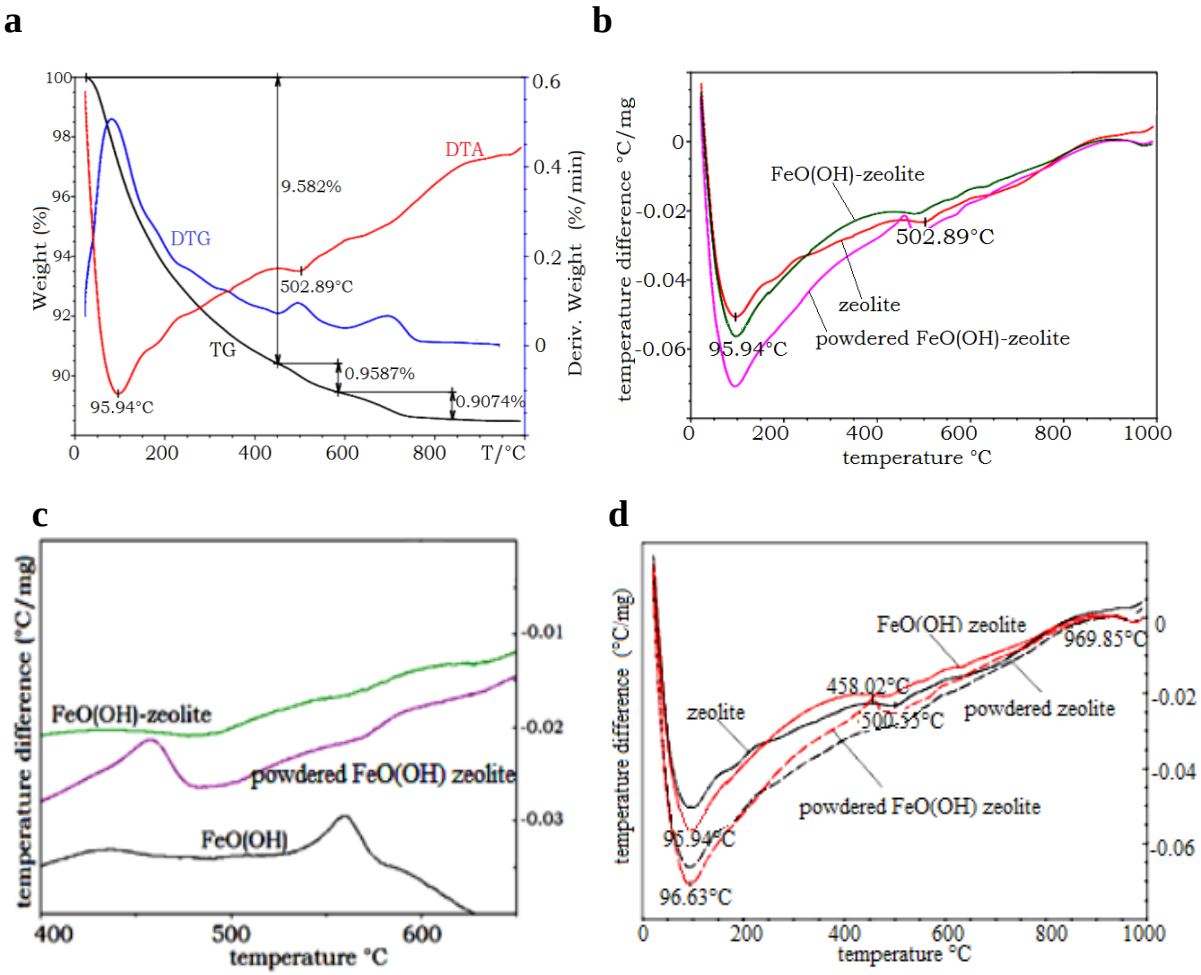

Fig. 7. Thermoanalytical curves - TG and DTG for both zeolite and FeO(OH) zeolite samples show qualitative similar course with 3 degrees of weight uptake (a); DTA differential thermal analysis of

individual samples, showing enhanced intensity of endothermic peak in the range 900 – 1000°C for FeO(OH) zeolite and a new maximum at 400-500°C for its powdered sample appeared (b); DTA curves clearly show the exothermic maximum at 560°C for FeO(OH) and for powdered FeO(OH) zeolite at 460°C (c); DTA curves for both raw and FeO(OH) zeolite grain-sized 0.2-0.5 mm and its powdered form (d).

3.2. Sb adsorption

According to some authors [7,8,10,18,20] amorphous extra framework Fe species might be deposited on both internal and external surface of zeolite rock in its FeO(OH) modification. The metallic sites are probably constituted by isolated species like $(Fe\text{-}O\text{-}Fe)^{4+}$, $(FeO)^{+}$ or binuclear clusters $[HO\text{-}Fe\text{-}O\text{-}Fe\text{-}OH]^{2+}$ [21,22]. These species are bound to the framework via one or two oxo-ions and can compensate one or two negative charges of the zeolite lattice depending on the number of OH groups coordinating the iron cations. In FeO(OH) zeolite rock, basically Fe^{3+} cation may compensate three spatially separated negative charges of AlO_4^{5-} tetrahedra. Some small amount of these cations might be localized at cationic sites and additional most likely form some iron oxo- or hydroxo-complexes undergoing during the synthesis various chemical transformation. However, considerably part of Fe neutral species as well ionic clusters are probably deposited outside zeolite framework because clinoptilolite structure contains channels with the size of 0.33 × 0.46 nm; 0.3 × 0.76 nm and 0.26 × 0.47 nm not sufficient large for their entrance [12,21]. They might associate then with ion-exchange reactions or surface complexation which occur through the removal or the addition of hydrogen atom. Due to strongly basic conditions during the synthesis of FeO(OH) zeolite, the surface groups lose their hydrogen ions and became negatively charged where Fe^{3+}ions may be localized by forming various Fe species as aforementioned. Species in form of hematite Fe_2O_3 and other Fe(III) oxides were also confirmed by XPS, FTIR and Raman spectroscopy in this study. Based on the thermoanalytical studies strong interactions between FeO(OH) species and zeolite rock was observed, too. A broad variety of physically and chemisorbed Fe species in zeolite rock may serve then in enhanced $Sb(OH)_3$, SbO^{+}, $Sb(OH)_2^{+}$, H_3SbO_4 and H_3SbO_3 uptake via intercalation, electrostatic interaction and other sorption processes. According to Table 2 FeO(OH) zeolite rock posses sufficient large mesopores (average pores diameter BJH 13.8 nm) for intercalation of Sb species also inside the internal surface.

Conventional Freundlich and Langmuir isotherms were used to fit the experimental data. The variation of the extent of adsorption with concentration of solutes in Fig. 8 illustrate that the adsorbents provide high solute uptake capacity at higher initial concentration. The Langmuir isotherm predicts a surface with homogenous binding sites, equivalent sorption energies and any interaction between attended entities. In mathematical equation used to be written as:

$$\frac{1}{a} = \left(\frac{1}{a(\max).b.c(eq)} \right) + \left(\frac{1}{a(\max)} \right)$$

where a means the specific solute uptake capacity,
a(max) the maximum adsorption capacity in mg/g,
c(eq) the equilibrium concentration in solution in mg/L and
b relates to the affinity of the solute for the binding sites expressed in L/mg.

The Freundlich isotherm is an empirical equation based on an exponential distribution of adsorption sites and energies and its form is represented as:

$$a = K.c(eq)^{\frac{1}{n}}$$

$$\log a = \log K + \frac{1}{n}\log c(eq)$$

where K and 1/n are related terms to the adsorbent capacity and adsorption intensity, respectively. Nevertheless, both Langmuir and Freundlich isotherms represent as well as follows the data satisfactorily, the Langmuir model seems better to fitt. The computed values of Langmuir and Freundlich constants using the statistical least square method *(MW XP, Microsoft Office Excel 2003, Regression Analysis*) are tabelled (Tab.4). The Langmuir parameter b predicts the affinity of adsorbate vs. adsorbent as dimensionless separation factor f(s):

$$f(s) = \frac{1}{(1 + b.c_0)}$$

where c_0 is the initial solute concentration in mg/L and b is the Langmuir adsorption equilibrium constant in L/mg.

If the f(s) values are equal to zero or one, the adsorption is either linear or irreversible and if the values are in between zero and one, adsorption is favourable to chemisorption. Our values can be situated between 0 and 1, what means that the proces was always favourable. All adsorption isotherms were carried out at the laboratory temperature 23 ± 0.2 °C.

Table 4
Freundlich and Langmuir isotherm´s data of system studied.

Adsorbent	Langmuir isotherm			Freundlich isotherm		
	a_{max} (mg/g)	b (L/mg)	R^2	n	K (L/mg)	R^2
GEH	18.58	7.64	0.8699	6.20	12.94	0.8545
FeO(OH)	7.15	0.02	0.9397	1.14	1.19	0.9415
FeO(OH) zeolite	7.17	0.81	0.9891	1.41	0.70	0.9930
Nanofer 25S	4.16	1.13	0.5213	3.71	1.77	0.8989

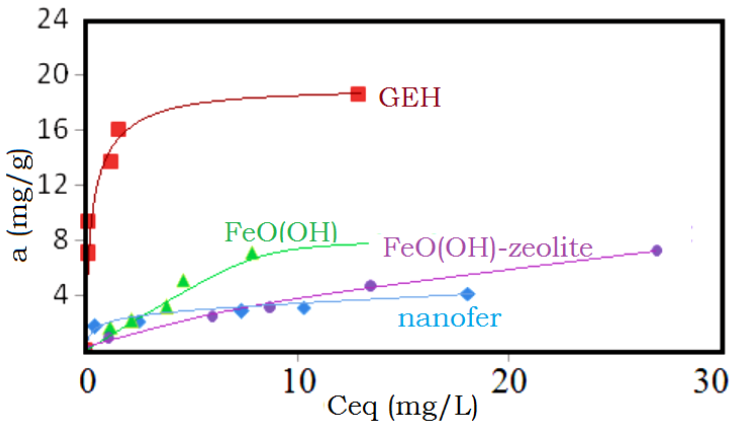

Fig. 8. Adsorption isotherms for aqueous Sb species uptake on the GEH, FeO(OH), FeO(OH) - zeolite and nanofer.

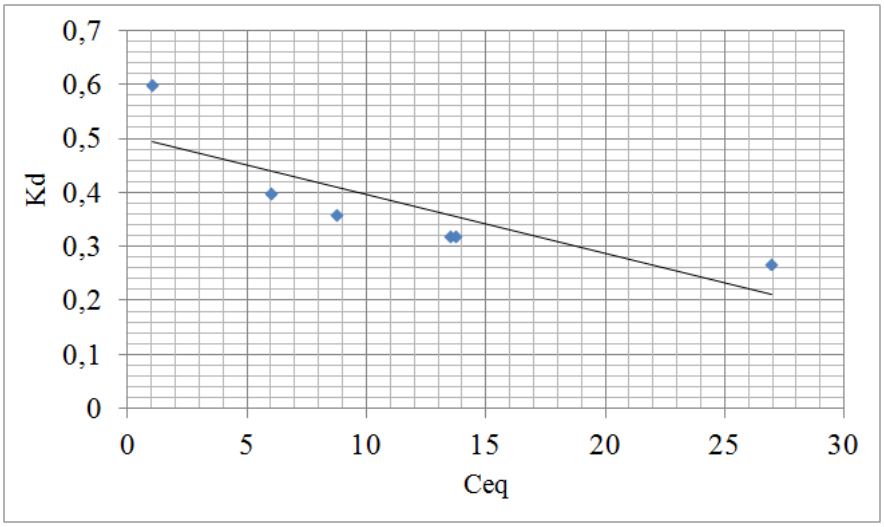

Fig. 9. Dependance of Kd versus Ceq in Sb solutions for FeO(OH) zeolite.

Finally, the adsorption ability of all examined adsorption materials towards Sb species in aqueous solutions was compared (Fig. 8). In highly acidified solutions (pH < 2.7) antimony is predominantly dissolved in Sb(III) valency as $Sb(OH)_3$, SbO^+, $Sb(OH)_2^+$ and H_3SbO_3 [19,20]. The plotting of adsorption isotherms in the system studied (Fig.8) clearly confirmed the increasing uptake capacity of the adsorbents with the increased S(BET) data. As aforementioned, the highest surface area possess GEH, then ferrihydrite, followed by FeO(OH) zeolite, whereas the lowest surface area belongs to nanofer (according to the Table 2 is S(BET) of nanofer 25 $m^2.g^{-1}$). Thus, FeO(OH) doped zeolite enriched its internal and external surface mostly with complexation centers which are active for antimony removal. Probably this fact together with mesoporous nature of the tuff and thus plenty of accessible space with much broader external pore openings and various interparticle voids contributed to its increased ability for antimony uptake. As seen in Fig.8, embedding FeO(OH) onto zeolite rock lowered its adsorption capacity towards antimony. Nevertheless at the higher equilibrium concentrations adsorption plateau of FeO(OH) zeolite reached comparable values of a(max) with pure FeO(OH) component. Fig.9 displays Kd (distribution coefficient) versus Ceq (Sb equilibrium concentrations) for FeO(OH) zeolite, which despite its isotherm in Fig.8 did not assign fully linear tendency of Kd lowering with Ceq increasing but the dependence seems to converge slowly to some fix Kd value. This phenomenon indicates a gradual saturation of FeO(OH) zeolite with antimony.

4. Conclusions

Metal oxides such as iron oxide are natural, low cost adsorbents for aqueous pollutants removal, however their nanoscale counterparts with higher specific surface area must be usually compressed into porous pellets or to be impregnated onto some carriers (like zeolite) to achieve better filtration performance.

Therefore, we prepared and thoroughly investigated iron oxide nano-particles embedded onto the Slovakian clinoptilolite tuff which based on its nano-porous structure worked as a nano-reactor.

Following conclusions were stated:

(1) The new synthesized FeO(OH) zeolite enriched the Fe content in regard to its parent (raw) zeolite based on SEM-EDS analyses more than 6 times, what was enough for Sb removal. Raw zeolite did not remove any antimony (or very negligible) from aqueous solutions.
(2) Mostly amorphous extra framework Fe species might be deposited on both internal and external surface of zeolite rock in its FeO(OH) modification working probably as complexation centers. Mesoporous nature of the zeolite rock (BJH 13.8 nm) with plenty accessible space and much broader external pore openings and various interparticle voids than clinoptilolite structure with the pore size of 0.33 × 0.46 nm; 0.3 × 0.76 nm and 0.26 × 0.47 nm provided inside them during above synthesis extensive FeO(OH) dispersion and thus contributed to its increased ability for antimony removal.
(3) After the treatment of raw zeolite with highly alkalic iron nitrate solutions, the XRD measurements did not reveal any clinoptilolite matrix destruction.
(4) According to Raman spectroscopy the spectra of FeO(OH) zeolite, GEH and oxidized nanofer, except FeO(OH), remained quite similar. Characteristic bands near 670 cm^{-1} and 300 cm^{-1} may be assigned to magnetite and bands around 600, 400, 280 and 220 cm^{-1} to hematite. IR spectroscopy confirmed also appearance of hematite in FeO(OH) zeolite.
(5) SEM micrographs of FeO(OH) zeolite revealed small inclusions filled with iron oxides, while some crystal habits of iron oxide were seen round or disc-shaped hematite coordinating rod-shaped goethite beside the main flacke-like ferrihydrite. TEM micrographs confirmed appearence of some clusters of Fe species outside the clinoptilolite crystals.
(6) There were confirmed also differences between Fe species in the raw and FeO(OH) zeolite in increasing surface Si/Al ratio, measured as 3.94 for raw and 5.38 for sample treated with alkalic solution, however based on XPS technique only below approximately 5 nm from the outer surface. Some small Al leaching (0.14 wt.%) may not be excluded due to alkalic treatment of zeolite. Oppositely, according to SEM-EDS values, the bulk Si/Al ratio dropped from 5.3 to 4.98.
(7) Thermoanalytical curves - TG and DTG for both zeolite and FeO(OH) zeolite samples showed qualitative similar course with 3 degrees of weight uptake. Supposing that doped Fe(III) element substitutes Al(III) atom in AlO_4^{5-} - tetrahedras of zeolite matrix or destroyed some surface AlO_4^{5-} - tetrahedras, the crystal structure of FeO(OH) zeolite started to break down earlier at the temperature 458.02°C. Also 2 recorded exothermic maxima on DTA curves, for powdered FeO(OH) zeolite at 460°C and for pure component FeO(OH) at 560°C, indicated an 100°C shifted exothermic effect, which characterized strong chemical interaction of FeO(OH) with zeolite structure.
(8) The plotting of adsorption isotherms in the system studied clearly confirmed the increasing uptake capacity of the adsorbents with the increased S(BET) data (GEH >FeO(OH)>FeO(OH) zeolite>nanofer).
(9) Main advantages of Sb removal by using of FeO(OH) zeolite might be the relatively low capital costs and therefore applicability to a large volume of waters, especially to highly acidic mine waters. Domestic clinoptilolite tuff is available in the local market for the price which is approx. 100 times lower that the price of commercial GEH product.

References

[1] E. Jabbari (Ed.), Handbook of Biomimetics and Bioinspiration. 1 Bioinspired Materials. (World Scientific Series in Nanoscience and Nanotechnology, Volume 9) World Scientific Publishing Co. Pte Ltd., Singapore 2014.
[2] Y. Zhou (Ed.), Bio-Inspired Nanomaterials and Nanotechnology. Nova Biomedical Books. Nova Science Publ. Inc., New York 2010.

[3] V. Mittal (Ed.), Advances in Polymer Nanocomposite Technology, Nova Science Publ. Inc., New York 2010.
[4] E. Chmielewská, F. Xu, Current Green Chemistry 2,4 (2015) 362-370.
[5] S. C.N. Tang, I. M.C. Lo, Water Research 47 (2013) 2613-2632.
[6] A. Subramani, J. G. Jacangelo, Water Research 75 (2015) 164-183.
[7] M. Akgül, J. Hazard. Materials 267 (2014) 1-8.
[8] M. K. Doula, Water Research 43 (2009) 3659-3672.
[9] E.A. Favret, N.O. Fuentes (Ed.), Functional Properties of Bio-Inspired Surfaces**,** Characterization and Technological Applications, © World Scientific Publishing Co. Pte. Ltd. 2009.
[10] M. Šiljeg, Š.C. Stefanivič, M. Mazaj, N.N. Tušar, I. Arčon, J. Kovač, K. Margeta, V. Kaučič, N. Zabukovec Logar, Microporous Mesoporous Mat. 118(2009) 408-415.
[11] R. Watkins, D. Weiss, W. Dubbin, K. Peel, B. Coles, T. Arnold, J. Colloid Interface Sci. 303 (2006) 639-646.
[12] E. Chmielewská, Comprehensive Guide for Mesoporous Materials, Vol. 4: Application and Commercialization, Mahmood Aliofkhazraei (Ed.) NOVA Science Pbl. Inc. NY (USA) 2015.
[13] X, Qu, P.J.J. Alvarez, Q. Li, Water Research 47 (2013) 3931-3946.
[14] G. Ungureanu, S. Santos, R. Boaventura, C. Botelho, J. Environ. Manag. 151 (2015) 326-342.
[15] A. Jaiswal, S. Banerjee, R. Mani, M.C. Chattopadhyaya, J. Environ. Chem. Eng. 1(2013) 281-289.
[16] Z. Swiatkowska-Warkocka, K. Kawaguchi, H. Wang, Y. Katou, N. Kozhizaki, Nanoscale Research Lett. 6 (2011) 226-233.
[17] Y. S. Li, J. S. Church, A. L. Woodhead, J. Magnetism Magnetic Mat. 324 (2012) 1543-1550.
[18] D. Ruiz-Serrano, M. Flores-Acosta, E. Conde-Barajas, D. Ramirez-Rosales, J.Yanez-Limon, R. Ramirez-Bon, J. Molecul. Struc. 980 2010)149-155.
[19] R. Jing-Hua, M. Lena Q., S. Hong-Jie, C. Fei, L. Jun, Science Total Environ. 475 (2014) 83-88.
[20] J. M. Casas, G. Crisostomo, L. Cifuentes, The Canadian J. Chem. Eng. 82 (2004) 175-183.
[21] E.A. Urquieta-Gonzalez, L. Martins, R.P.S. Peguin, M.S. Batista, Materials Research 5 (2002) 321–327.
[22] E.M. El-Malki, R.A.Van Santen, W.M.H. Sachtler, Journal of Physical Chemistry B 103(1999) 4611–4622.

Acknowledgment

This project is supported by the APVV agency of Slovakia under the code: SK-SRB-2015-0001 – Zeolite-based adsorbents for environmental remediation. The authors thank for financial support. The publication is also a result of project implementation: Development and application of advanced diagnostic methods in the processing of metallic and non-metallic materials - APRODIMET, ITMS: 26220120048 supported by Research & Development Operational Programme funded by the ERDF and also by Slovak Ministry of Education within the Programme "University Science Park of STU Bratislava" and co-funded by the European Regional Development Fund (ITMS 26240220084).